Research Square

Preprints are preliminary reports that have not undergone peer review.
They should not be considered conclusive, used to inform clinical practice,
or referenced by the media as validated information.

HMGB1 Mediates Hepatic Ferroptosis and Fibrosis Triggered by Echinococcus granulosus Infection

Shaohua Zhai

183099169370163.com

Xinjiang Agricultural University

Songhan Liu

Xinjiang Agricultural University

Laizhen Liu

Xinjiang Agricultural University

Meihe Hu

Yili Chuanning Biotechnology Co., Ltd

Yueqi Yang

Xinjiang Agricultural University

Jiahao Zhai

Xinjiang Agricultural University

Xiaoying Wei

Xinjiang Agricultural University

Jingjing Yao

Xinjiang Agricultural University

Research Article

Keywords: Echinococcus granulosus, liver injury, HMGB1, ferroptosis, liver fibrosis

Posted Date: November 5th, 2026

DOI: https://doi.org/10.21203/rs.3.rs-11429768/v1

License: This work is licensed under a Creative Commons Attribution 4.0 International License.
Read Full License

Additional Declarations: No competing interests reported.

HMGB1 Mediates Hepatic Ferroptosis and Fibrosis Triggered by *Echinococcus granulosus* Infection

Shaohua Zhai [1,2*,†], Songhan Liu [1,2,†], Laizhen Liu [1,2], Meihe Hu [3], Yueqi Yang [1,2], Jiahao Zhai [1,2], Xiaoying Wei [1,2], Jingjing Yao [1,2]

1 College of Veterinary Medicine, Xinjiang Agricultural University, Urumqi 830052, China;

2 Xinjiang·Key Laboratory of New Drug Research and Development for Herbivorous (XJ-LNDRDH), Urumqi 830052, China;

3 Yili Chuanning Biotechnology Co., Ltd, Yili 835000, China.

*Corresponding author(s). E-mail(s): 18309916937@163.com;

Contributing authors: 18309916937@163.com; a807953546@2980.com; liu859lsqc@163.com; 17881123623@163.com; yangyueqi7788@163.com; 18146925749@163.com; Weixxiy2023@163.com; 18703021672@163.com

†These authors contributed equally to this work.

Abstract: (1) Background: Cystic echinococcosis (CE), caused by *Echinococcus granulosus*(*E. granulosus*), is a globally distributed zoonosis predominantly affecting the liver. Persistent infection provokes chronic inflammation, hepatocellular injury, and fibrotic cyst formation, yet the molecular mechanisms remain incompletely defined. High-mobility group box 1 (HMGB1), a damage-associated molecular pattern, regulates inflammation, oxidative stress, and ferroptosis. This study investigated whether HMGB1 coordinates an inflammation-ferroptosis-fibrosis axis during *E. granulosus*-induced liver injury. **(2) Methods:** We examined HMGB1 using liver tissues from naturally infected sheep, an infected rat model, and in vitro BRL hepatocytes and HSC-T6 stellate cells. Histopathological injury, collagen deposition, and iron accumulation were assessed by staining. HMGB1, Fe^{2+}, lipid peroxides, glutathione, superoxide dismutase, and malondialdehyde were quantified, and ferroptosis-, inflammation-, and fibrosis-related proteins were analyzed. Glycyrrhizic acid (GA) and ferrostatin-1 (Fer-1) were

used for intervention. **(3) Results:** Infection increased HMGB1 expression and release, promoted hepatic iron accumulation and lipid peroxidation, impaired antioxidant defenses, downregulated GPX4 and SLC7A11, and upregulated TFRC. It also activated TLR4/MYD88 and TGF-β/Smad signaling, induced hepatic stellate cell activation, and enhanced collagen deposition. Iron-positive regions overlapped with fibrotic areas. Inhibition of HMGB1 or ferroptosis corrected iron-metabolism abnormalities, attenuated oxidative stress, and suppressed inflammatory and fibrotic responses; GA exerted broader protection. Exogenous HMGB1 further aggravated hepatocyte ferroptosis and promoted stellate activation. **(4) Conclusions:** HMGB1 functions as an upstream regulator linking *E. granulosus*-induced injury to ferroptosis, inflammation, and fibrosis. Targeting HMGB1 or ferroptosis may represent a promising therapeutic strategy for hepatic CE.

Keywords: *Echinococcus granulosus*; liver injury; HMGB1; ferroptosis; liver fibrosis

1 Introduction

Cystic echinococcosis is a widespread zoonotic disease caused by infection with Echinococcus granulosus in humans and other mammals[1,2]. The disease is endemic in more than 100 countries, particularly in pastoral regions of temperate, subtropical, and cold climates, and continues to impose a substantial burden on public health and livestock production[3-9]. The liver is the principal target organ[10,11]. Persistent exposure to parasite-derived products and the expanding hydatid cyst initiates chronic inflammation, hepatocellular injury, inflammatory-cell infiltration, and excessive extracellular matrix deposition, ultimately leading to hepatic fibrosis and, in severe cases, liver failure[12-16]. Our previous work showed that *E.granulosus* protoscoleces(PSC) disrupt hepatic iron homeostasis, induce oxidative stress, and trigger hepatocyte ferroptosis. Pharmacological inhibition of ferroptosis with Fer-1 attenuated liver injury and reduced cyst

formation in both in vivo and in vitro models[17-19]. Nevertheless, the upstream signals that initiate ferroptosis during infection, and the extent to which this process contributes to parasite growth and fibrogenesis, remain unclear.

High-mobility group box 1 (HMGB1) is a prototypical damage-associated molecular pattern and a central mediator of sterile inflammation and tissue injury[20,21]. During *E.granulosus*-infection, mechanical compression by hydatid cysts, parasite-derived toxic products, and direct cellular injury may promote the passive release of nuclear HMGB1 from damaged hepatocytes, together with Fe^{2+} and lactate dehydrogenase[22-27]. Extracellular HMGB1 can amplify oxidative stress and regulated cell death, including ferroptosis[28,29]. Conversely, ferroptotic membrane damage may further enhance HMGB1 release, thereby establishing a self-reinforcing cycle of cellular injury and inflammation[30,31]. HMGB1 also engages pattern-recognition receptors on macrophages, neutrophils, and other immune cells, stimulating the production of IL-6, TNF-alpha, and IL-1beta and activating inflammatory pathways such as NF-kappaB, JAK/STAT3, and MAPK[32]. Sustained inflammatory signaling can activate hepatic stellate cells (HSCs), promote extracellular matrix synthesis, and accelerate the progression of liver fibrosis[33,34]. These observations suggest that HMGB1 may occupy a critical mechanistic position at the intersection of ferroptosis, inflammation, and fibrogenesis.

Accordingly, the present study examined the role of HMGB1 in E. granulosus-induced liver injury using complementary naturally infected, experimental animal, and cell-culture models. We characterized HMGB1 expression and release within the infected hepatic microenvironment and assessed its relationship with iron dysregulation, oxidative stress, ferroptosis, inflammatory signaling, HSC activation, and collagen deposition. Pharmacological inhibition of HMGB1 and ferroptosis was then used to define the directionality of these interactions. The results identify HMGB1 as an upstream

regulator of an inflammation-ferroptosis-fibrosis cascade and provide a mechanistic basis for therapeutic strategies targeting the host response in hepatic CE.

2 Materials and Methods

2.1 Ethical Approval

All animal experimental protocols were reviewed and approved by the Animal Experiment Ethics Committee of Xinjiang Agricultural University (Approval ID: 2022039).

2.2 Experimental Animals and Parasite Isolation

2.2.1 Naturally Infected Sheep Liver Samples

Sheep livers naturally infected with one or more whitish hydatid cysts containing viable protoscoleces were collected from slaughterhouse-discarded tissues in the Urumqi region. Livers from routinely slaughtered sheep without visible cystic lesions were used as healthy controls, and blood samples were collected and tested negative using a blocking ELISA kit for ovine echinococcosis.*Echinococcus* blocking ELISA antibody detection kit (Lot No.: EG-EB 2501, Beijing Tianzhitai) and used according to the manufacturer's instructions.

2.2.2 Sprague-Dawley (SD) Rats

Male SD rats (80 ± 5 g) were purchased from the Experimental Animal Center of Xinjiang Medical University. Animals were housed in clean cages under controlled temperature and humidity with a 12 h light/dark cycle and provided with standard rodent chow and purified water ad libitum.

2.2.3 Isolation of *E. granulosus* protoscoleces

E. granulosus protoscoleces were isolated from hydatid cysts in the livers of naturally infected sheep.Cyst fluid was aspirated, allowed to settle, and washed repeatedly with phosphate-buffered saline (PBS) containing 1% penicillin–streptomycin. Viability

was assessed by trypan blue exclusion, and only preparations with viability ≥ 90% were used.

2.3 Establishment of a Rat *E. granulosus* Infection Model

The protoscolex suspension was concentrated and adjusted to a concentration of 2 ×10⁴ PSCs/mL. Sprague-Dawley (SD) rats were anesthetized by intraperitoneal injection of pentobarbital sodium (50 mg/kg), and a laparotomy was performed to fully expose the liver. A 1 mL sterile syringe was used to aspirate 0.5 mL of the protoscolex suspension, which was then slowly injected into the right hepatic lobe at a depth of approximately 1 cm with a 45° insertion angle. After injection, the puncture site was pressed with a sterile dry cotton swab to achieve hemostasis. The control group underwent a sham operation, receiving an equivalent volume of 0.9% sterile saline injected into the liver. Subsequently, 1 mL of procaine penicillin in oil was injected into the peritoneal cavity, the abdominal wall was sutured layer by layer, and the rats were allowed to recover from anesthesia and maintained under standard housing conditions for observation.

2.4 Experimental design and animal grouping

SD rats were randomly assigned to four groups: (1) Control group, receiving an intrahepatic injection of 0.5 mL sterile saline; (2) *E. granulosus* model group, receiving an intrahepatic injection of 0.5 mL protoscolex suspension (2 × 10⁴ PSCs/mL); (3) *E. granulosus* + Fer-1 group, receiving intraperitoneal Fer-1 (5 mg/kg once daily for 21 consecutive days); and (4) *E. granulosus* + GA group, receiving intraperitoneal GA (100 mg/kg once daily for 21 consecutive days). GA (purity ≥ 98% by HPLC) was purchased from Shanghai Yuanye Biotechnology Co., Ltd. (Shanghai, China; catalog no. B20418). All animals were euthanized 1 month after infection, and serum and liver tissues were collected for subsequent analyses.

2.5 Cell Culture and *in vitro* Models

Rat BRL hepatocytes (Cat. No.CL-0038) and HSC-T6 hepatic stellate cells (Cat. No. CL-0116) were obtained from Procell Life Science & Technology Co., Ltd. (Wuhan, China) and cultured in RPMI-1640 medium supplemented with 10% fetal bovine serum and 1% penicillin–streptomycin at 37℃ in a humidified 5% CO_2 incubator. To assess hepatocyte-HSC crosstalk, BRL cells were exposed to *E. granulosus* protoscoleces or treated with recombinant HMGB1, ferrostatin-1 (Fer-1), or glycyrrhizic acid (GA) as indicated. Conditioned medium from treated BRL cells was transferred to HSC-T6 cells, and recombinant HMGB1 was also applied directly to HSC-T6 cells.

2.6 Histopathological Examination

Liver tissues were fixed in 4% paraformaldehyde, embedded in paraffin, and cut into 5-μm sections. Hematoxylin and eosin (H&E), Masson's trichrome, and Prussian blue iron staining were performed to evaluate hepatic histopathological changes, collagen deposition, and iron accumulation, respectively.

2.7 HMGB1 measurement

HMGB1 concentrations in serum, cell culture supernatants, and liver tissue homogenates were determined using a commercial ELISA kit (catalog no. CSB-E08224r; Wuhan Huamei Biotech Co., Ltd. [CUSABIO], Wuhan, China) according to the manufacturer's instructions. Blood collected from the orbital sinus was centrifuged to obtain serum, and liver homogenates were centrifuged to collect supernatants. Standards and samples were added to 96-well plates, incubated with the supplied reagents, and developed colorimetrically. Absorbance was measured at 450 nm, and HMGB1 concentrations were calculated from the standard curve.

2.8 Fe^{2+} measurement

Fe^{2+} levels in liver tissues and BRL cells were quantified using a commercial kit (catalog no. BC5415; Beijing Solarbio Science & Technology Co., Ltd., Beijing, China). Tissue and cell homogenate supernatants were prepared, reagents were added according to the protocol, and the mixtures were incubated. After chloroform extraction and centrifugation, absorbance at 593 nm was recorded. Fe^{2+} concentrations were calculated from a standard curve.

2.9 Lipid peroxide (LPO) measurement

LPO levels in liver tissues and BRL cells were determined using a commercial kit (catalog no. A106-1-2; Nanjing Jiancheng Bioengineering Institute Co., Ltd., Nanjing, China). Supernatants were prepared, reagents were added, and the mixture was incubated. After centrifugation, absorbance was measured, and LPO concentrations were derived from a standard curve.

2.10 Measurement of GSH, SOD, and MDA

Glutathione (GSH) content (catalog no. A001-3-2; Nanjing Jiancheng Bioengineering Institute Co., Ltd., Nanjing, China), superoxide dismutase (SOD) activity (catalog no. A003-1-1; Nanjing Jiancheng Bioengineering Institute Co., Ltd., Nanjing, China), and malondialdehyde (MDA) level (catalog no. A003-1-1; Nanjing Jiancheng Bioengineering Institute Co., Ltd., Nanjing, China) in liver tissues and BRL cells were measured using the respective commercial kits. Supernatants were incubated with working reagents according to the manufacturers' instructions. After centrifugation, absorbance was measured at 586 nm for GSH, 450 nm for SOD, and 532 nm for MDA, and concentrations or activities were calculated accordingly.

2.11 Western blot

Total protein was extracted from liver tissue homogenates and BRL cell lysates using RIPA lysis buffer (catalog no. AR0105; Bioss Biological Technology Co., Ltd.,

Beijing, China) supplemented with protease and phosphatase inhibitor cocktails (catalog no. AR1178; Bioss Biological Technology Co., Ltd., Beijing, China). Protein concentrations were determined by BCA assay. Equal amounts of denatured protein were separated by SDS-PAGE and transferred onto 0.45 μm or 0.22 μm PVDF membranes (Millipore, Burlington, MA, USA). Membranes were blocked with 5% non-fat milk or 5% bovine serum albumin in TBST for 1 h at room temperature and then incubated overnight at 4 °C with primary antibodies against collagen I (catalog no. bs-0578R; Bioss Biological Technology Co., Ltd., Beijing, China), GPX4 (catalog no. 67763-1-Ig; Proteintech, Wuhan, China), SLC7A11 (catalog no. 26864-1-AP; Proteintech, Wuhan, China), TFRC (catalog no. PB9233; Boster Biological Technology Co., Ltd., Wuhan, China), FTH1 (catalog no. BM4487; Boster Biological Technology Co., Ltd., Wuhan, China), TLR4 (catalog no. bs-1021R; Bioss Biological Technology Co., Ltd., Beijing, China), MyD88 (catalog no. AF5195; Affinity Biosciences, Changzhou, China), α-SMA (catalog no. AF1032; Affinity Biosciences, Changzhou, China), Smad2/3 (catalog no. AF6367; Affinity Biosciences, Changzhou, China), phosphorylated Smad2/3 (catalog no. AF3367; Affinity Biosciences, Changzhou, China), and β-actin (catalog no. 100166-MM10; Sino Biological Inc., Beijing, China). After washing three times with TBST, membranes were incubated with HRP-conjugated goat anti-rabbit IgG (catalog no. ab205718; Abcam, Cambridge, UK) or goat anti-mouse IgG (catalog no. ab205719; Abcam, Cambridge, UK) for 1 h at room temperature. Signals were visualized using an ultra-sensitive ECL chemiluminescence detection kit (catalog no. PK10003h; Wuhan Sanying Biotechnology Co., Ltd., Wuhan, China) and captured with a Chemiscope 3000 chemiluminescence imaging system (Shanghai Qinxiang Scientific Instrument Co., Ltd., Shanghai, China). Band intensities were quantified using ImageJ software, with β-actin as the loading control.

2.12 Statistical analysis

Data are presented as the mean±standard deviation. Statistical analyses were performed using SPSS version 26.0 and GraphPad Prism version 9.5. Comparisons between two groups were conducted using an independent-samples Student's t-test, whereas comparisons among three or more groups were performed by one-way analysis of variance followed by Tukey's post hoc test. A value of $P < 0.05$ was considered statistically significant. $P < 0.05$ and $P < 0.01$. Unless otherwise stated, experiments were independently repeated at least three times.

3 Results

3.1 HMGB1 Expression, Ferroptosis, and Fibrosis in Liver Tissues from Naturally Infected Sheep

Healthy sheep livers displayed a regular contour, smooth capsule, uniform reddish-brown parenchyma, and no visible structural abnormalities (Fig.1a, b). In contrast, livers naturally infected with *E. granulosus* exhibited irregular surfaces, distorted lobular architecture, and multiple milky-white to pale-pink cystic nodules surrounded by dense fibrous capsules (Fig.1c, d). The expanding lesions compressed and displaced the adjacent hepatic parenchyma. Prussian blue staining revealed no appreciable iron deposition in healthy livers (Fig.1e, f), whereas abundant iron-positive granules accumulated in hepatocytes surrounding hydatid cysts in infected tissues (Fig.1g-j).

Consistent with these histological findings, HMGB1 concentrations was significantly increased in both serum and liver homogenates from infected sheep(Fig.1k, l). Hepatic Fe^{2+} and lipid peroxide (LPO)levels were elevated, whereas GSH content and GPX4 expression were reduced(Fig.1m-q). Additionally, Western blot analysis demonstrated upregulated expression of the inflammatory receptor TLR4 and fibrosis-related markers, including TGFβR1, α-SMA, and COL1A1 (Fig.1r-v). These results indicate

that *E.granulosus*-infection is associated with iron accumulation, oxidative stress,and the activation of TLR4/TGF-β signaling pathways leading to liver fibrosis.

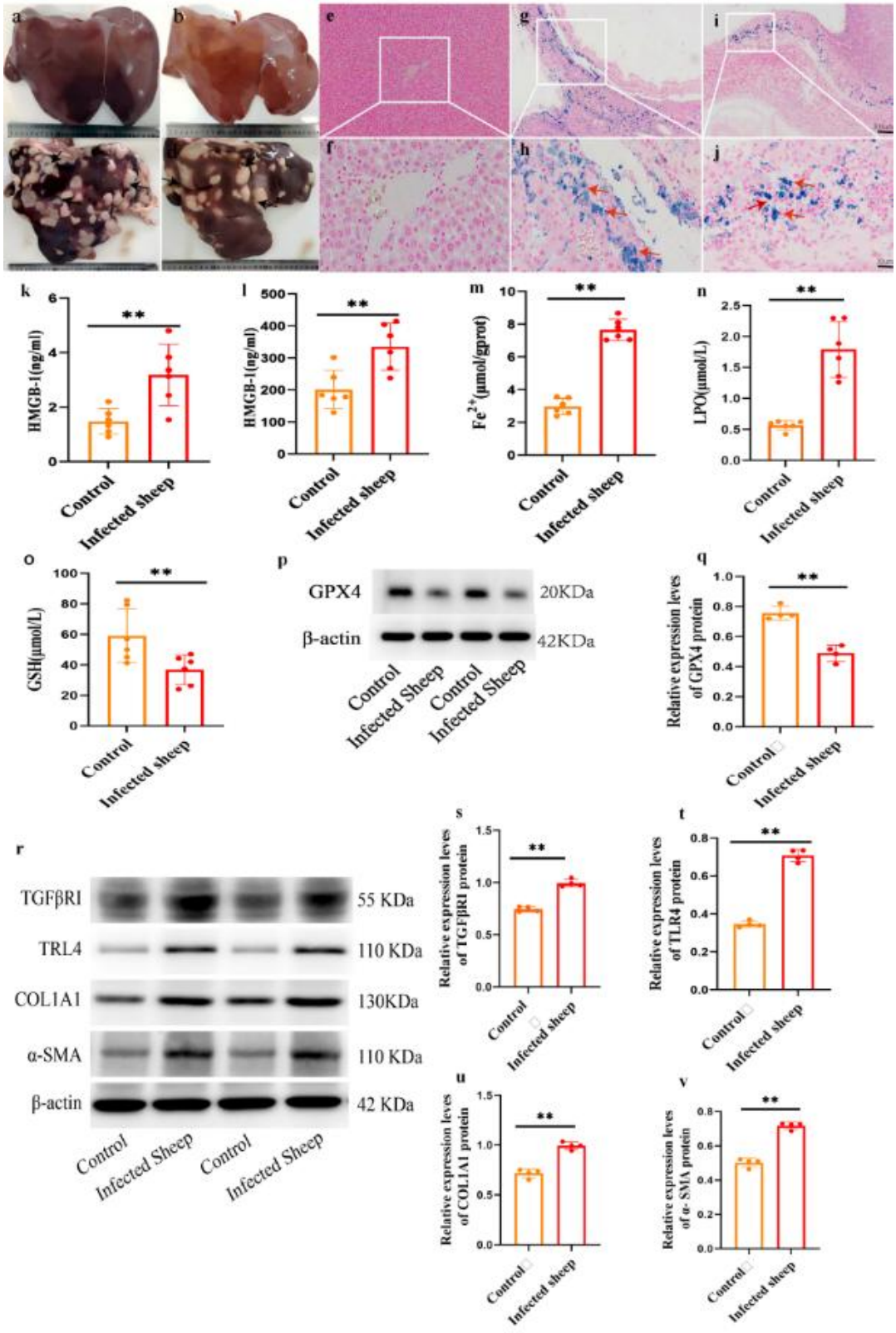


Fig 1. Gross anatomical and histopathological characterization of liver tissues from healthy and naturally *E. granulosus*-infected sheep.

(a,b): Representative macroscopic images of livers from healthy control sheep. (c,d): Macroscopic lesions of hydatid-infected sheep livers with abundant cystic nodules and surrounding fibrous capsules; black arrows indicate hydatid cysts. (e, f): Prussian blue iron staining of healthy sheep hepatic lobules. (g-j): Prussian blue staining of infected liver tissue around hydatid cysts; red arrows mark iron-positive granular deposits. Scale bars: 300 μm (low magnification) and 30 μm (high magnification). (k): Quantification of HMGB1 concentrations in serum homogenates. (l-o): Quantification of HMGB1, Fe^{2+}, LPO, and GSH concentrations in hepatic tissue homogenates. n = 6 per group. (p,q): Western blot band and quantitative analysis of ferroptosis marker GPX4.(r): Representative Western blot bands of fibrosis-related proteins (TGFBR1, TRL4, COLIA1, α-SMA). (s-v): Quantitative analysis of the relative protein expression levels corresponding to panel (r). n = 4 per group.

3.2 Protective Effects of Fer-1 and GA against Liver Injury in Rats Infected with *E. granulosus*

To evaluate the protective effects of ferroptosis and HMGB1 inhibition, infected rats were treated with Fer-1 or GA for 21 consecutive days. Livers from control rats were smooth, reddish, and free of visible nodules (Fig.2a), whereas those from untreated infected rats contained multiple cystic lesions of variable size(Fig.2b). Both Fer-1 and GA reduced the number and size of visible lesions and partially restored normal gross morphology (Fig.2c, d). Prussian blue staining showed extensive hepatic iron deposition in the infected group(Fig.2f1-2), which was markedly reduced by either intervention (Fig.2g1-h2). Hematoxylin and eosin and Masson's trichrome staining further demonstrated disrupted lobular architecture, inflammatory-cell infiltration, and

substantial collagen deposition in infected livers(Fig.2i1-j2). These abnormalities were attenuated in both treatment groups(Fig.2k1-p2). Across the evaluated histopathological features, GA produced a more pronounced improvement than Fer-1.

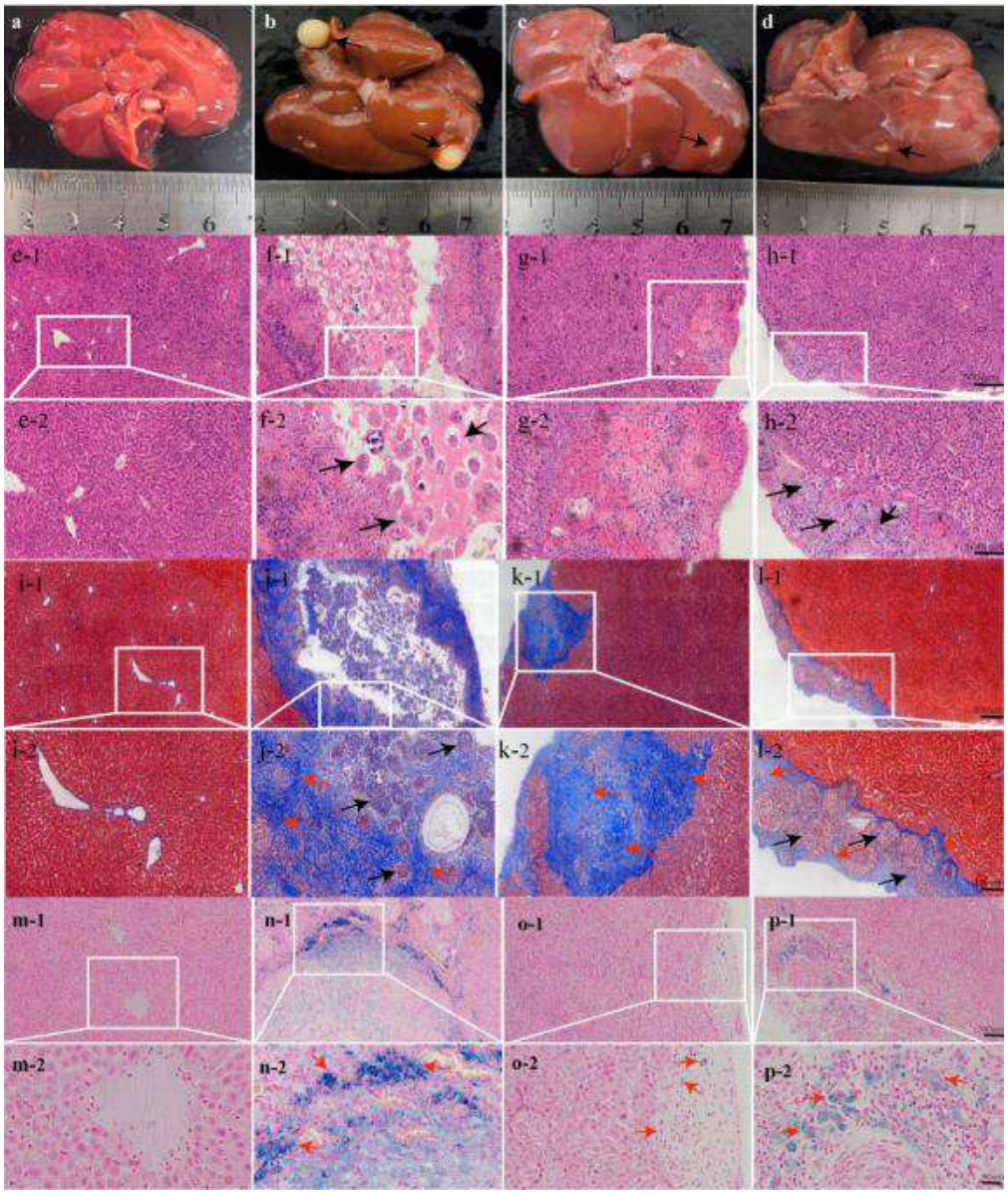


Fig 2. Representative images of liver gross morphology, histopathology, and iron deposition in SD rats one month after infection with *E. granulosus* protoscoleces, with or without daily treatment with Fer-1 or GA.

(a-d): Gross liver appearance. (a): normal control; (b): infected model showing multiple cysts (black arrows); infected rats treated with Fer-1 (c) or GA (d), both exhibiting fewer and smaller cysts. (e-h): H&E staining of liver sections from normal (e), infected

(f), infected+Fer-1 (g), and infected+GA (h) groups. For each group, two magnifications are presented (left column scale bar: 300 μm; right column scale bar: 100 μm). Black arrows indicate cysts. (i-l): Masson's trichrome staining of the corresponding groups (same magnifications and scale bars). Black arrows denote cysts; cyan arrows highlight fibrotic areas. (m-p): Prussian blue staining for iron deposition in normal (m), infected (n), infected+Fer-1 (o), and infected+GA (p) livers. Red arrows point to iron-positive deposits, which are abundant in the infected group but markedly reduced after either treatment. n = 6 per group.

3.3 HMGB1 Inhibitor Attenuates HMGB1 Secretion, Fe^{2+} Overload, and Oxidative Lipid Peroxidation in the Liver of *E. granulosus*-Infected Rats

To determine how infection and treatment affected iron metabolism and redox homeostasis, Fe^{2+}, lipid peroxides, HMGB1, GSH, SOD, and MDA were quantified in liver tissues. Relative to controls, infected rats exhibited increased Fe^{2+}(Fig.3a), lipid peroxide (Fig.3b), HMGB1 (Fig.3c), and MDA levels (Fig.3f), together with decreased GSH content(Fig.3d) and SOD activity (Fig.3e). These changes indicate that *E. granulosus*-infection induces hepatic iron accumulation, lipid peroxidation, and antioxidant depletion. Treatment with either Fer-1 or GA significantly reduced Fe^{2+}(Fig.3a), lipid peroxide(Fig.3b), HMGB1 (Fig.3c), and MDA levels(Fig.3f) and restored GSH (Fig.3d)and SOD (Fig.3e) toward control values. GA generally exerted a stronger corrective effect than Fer-1, particularly on HMGB1 release and iron accumulation.

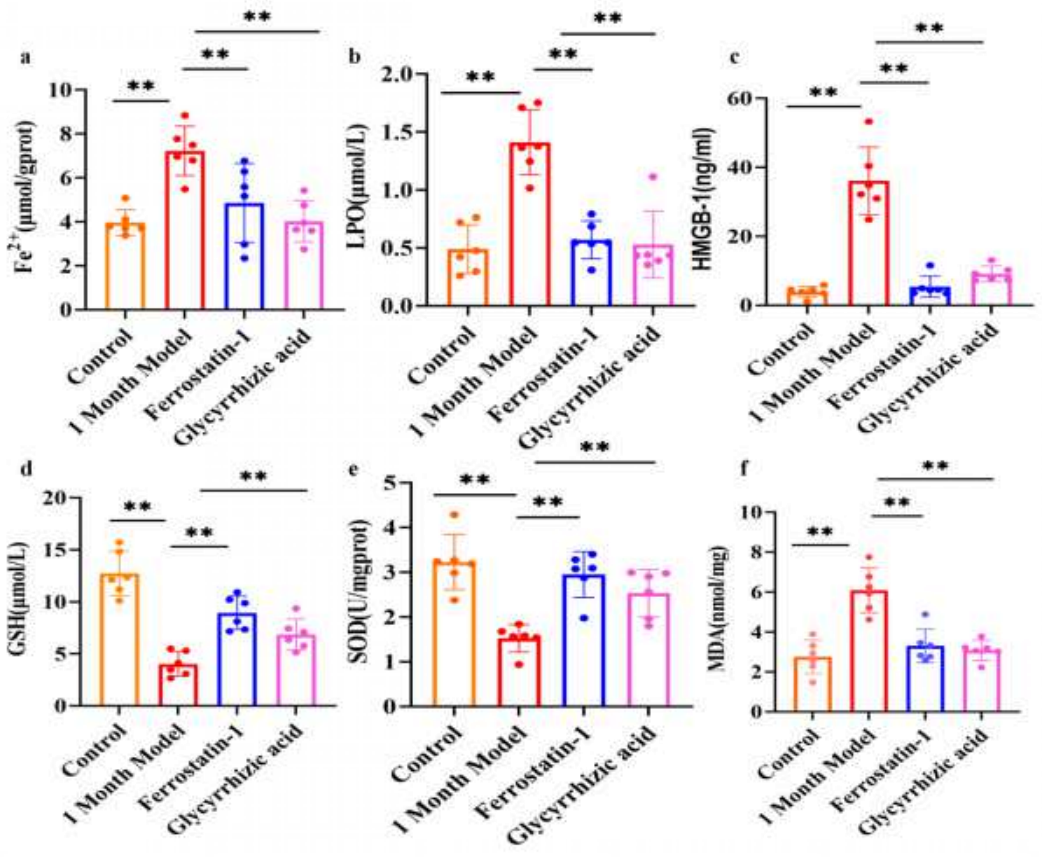


Fig 3. The effects of Fer-1 and GA treatments on the expression of iron accumulation and lipid peroxidation substances in liver cells of rats infected with *E. granulosus*. The expression levels of Fe^{2+}(a), LPO (b), HMGB1(c), GSH(d), SOD(e), and MDA(f) in hepatocytes from rats infected with *E. granulosus* in the different experimental groups. n = 6 per group.

3.4 HMGB1 Inhibition Alleviates Ferroptosis-Related Protein Expression in Liver Tissue of *E. granulosus*-Infected Rats

We next examined ferroptosis-related proteins in liver tissues (Fig.4a). Compared with controls, infected rats showed increased TFRC and FTH1 expression (Fig.4b, 4c) and reduced SLC7A11 (Fig.4d) and GPX4 expression (Fig.4e), consistent with enhanced iron uptake and impaired glutathione-dependent antioxidant defense. These molecular changes occurred in parallel with the reduction in GSH and SOD described above, supporting the induction of a pro-ferroptotic state. Both Fer-1 and GA partially

normalized the expression of TFRC, FTH1, SLC7A11, and GPX4 (Fig.4b–e). The effect was more pronounced in the GA-treated group, in which ferroptosis-related protein expression approached that observed in controls. These findings suggest that HMGB1 may play an upstream regulatory role in infection-associated ferroptosis.

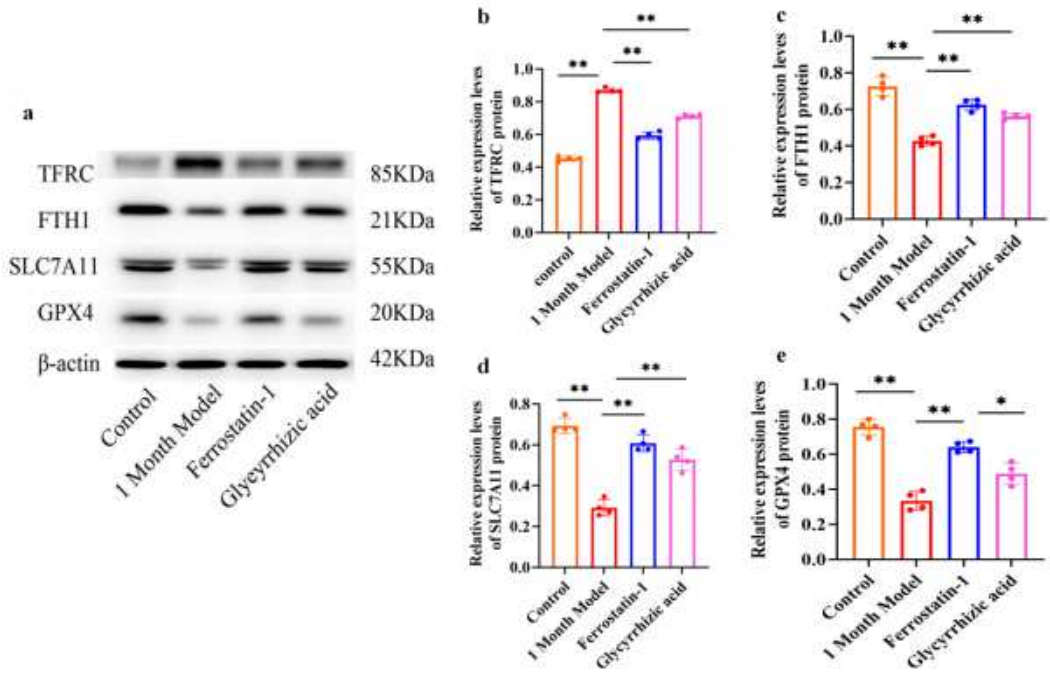


Fig 4. Expression of ferroptosis-related proteins in liver tissues from control and *E. granulosus*-infected rats treated with Fer-1 or GA.

(a): Representative Western blots of TFRC, FTH1, SLC7A11, and GPX4. Densitometric quantification of TFRC (b), FTH1 (c), SLC7A11 (d), and GPX4 (e) expression in each experimental group. n = 4 per group.

3.5 HMGB1 Inhibitor Reduces Fibrotic Protein Expression in Liver Tissue of *E. granulosus*-Infected Rats

To assess the relationship between HMGB1, inflammation, and fibrosis, we analyzed TLR4/MYD88 and TGF-β/Smad signaling in liver tissues. Infection markedly increased TLR4 (Fig.5f, g) and MYD88 expression (Fig.5f, h), indicating activation of the HMGB1-responsive inflammatory pathway. The abundance of phosphorylated

Smad2/3 was also increased (Fig. 5a, c), whereas total Smad2/3 remained largely unchanged (Fig.5a, d). In parallel, alpha-SMA (Fig.5a, b) and COL1A1 were upregulated (Fig.5a, e), consistent with HSC activation and enhanced collagen synthesis. Fer-1 reduced these inflammatory and fibrotic changes (Fig.5b-h), suggesting that ferroptosis contributes to pathway activation. GA produced a broader inhibitory effect, simultaneously suppressing TLR4/MYD88 signaling, Smad2/3 phosphorylation, alpha-SMA expression, and COL1A1 accumulation. Thus, direct HMGB1 inhibition attenuated both the inflammatory and fibrotic components of the hepatic response to infection.

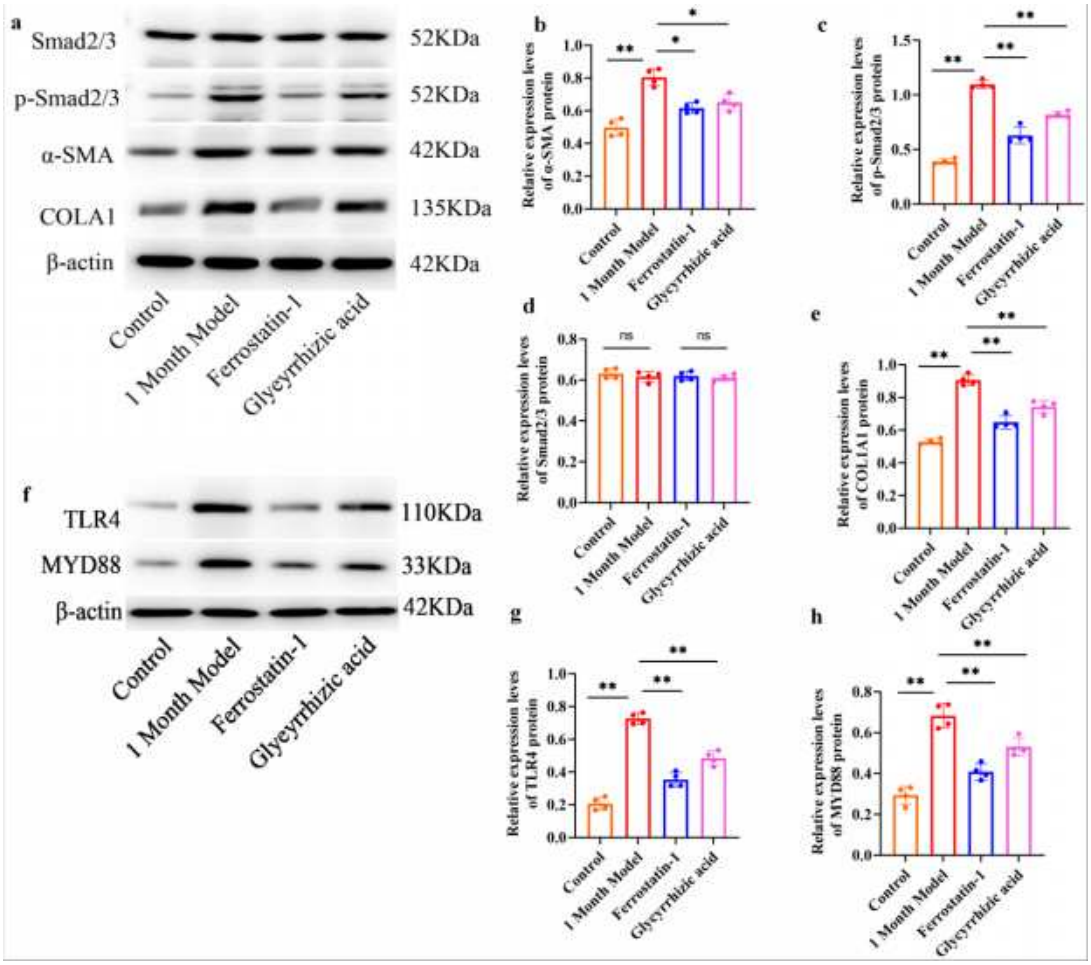


Fig 5. Protein expression levels of fibrosis-related markers (Smad2/3, phosphorylated Smad2/3, α-SMA, and COL1A1) and the TLR4/MYD88 signaling pathway in each group.

(a): Expressions of fibrosis-related proteins Smad2/3, p-Smad2/3, α-SMA and COL1A1 in each group. Quantitative analysis of α-SMA (b), p-Smad2/3 (c), Smad2/3 (d), COL1A1 (e), TLR4 (g) and MYD88 (h) protein expressions. (f): Expressions of TLR4 and MYD88 proteins in each group. n = 4 per group.

3.6 *E. granulosus* Infection Promotes HMGB1 Release from Hepatocytes and Activates Hepatic Stellate Cells

Exposure of BRL hepatocytes to PSCs caused cellular shrinkage and morphological injury (Fig.6a-e), whereas HSC-T6 cells exposed to hepatocyte-conditioned medium acquired an enlarged, elongated, and activated phenotype (Fig.6f-j). HMGB1 expression was increased in infected BRL cells (Fig.6k, l) and was further enhanced by exogenous recombinant HMGB1. Fer-1 and GA both reduced HMGB1 abundance (Fig.6k, l), with GA producing the greater effect. In parallel, inhibition of HMGB1 or ferroptosis mitigated iron accumulation and cellular injury and diminished the activation of HSC-T6 cells. These observations indicate that parasite-induced hepatocyte injury promotes HMGB1 release and generates a paracrine microenvironment capable of activating HSCs.

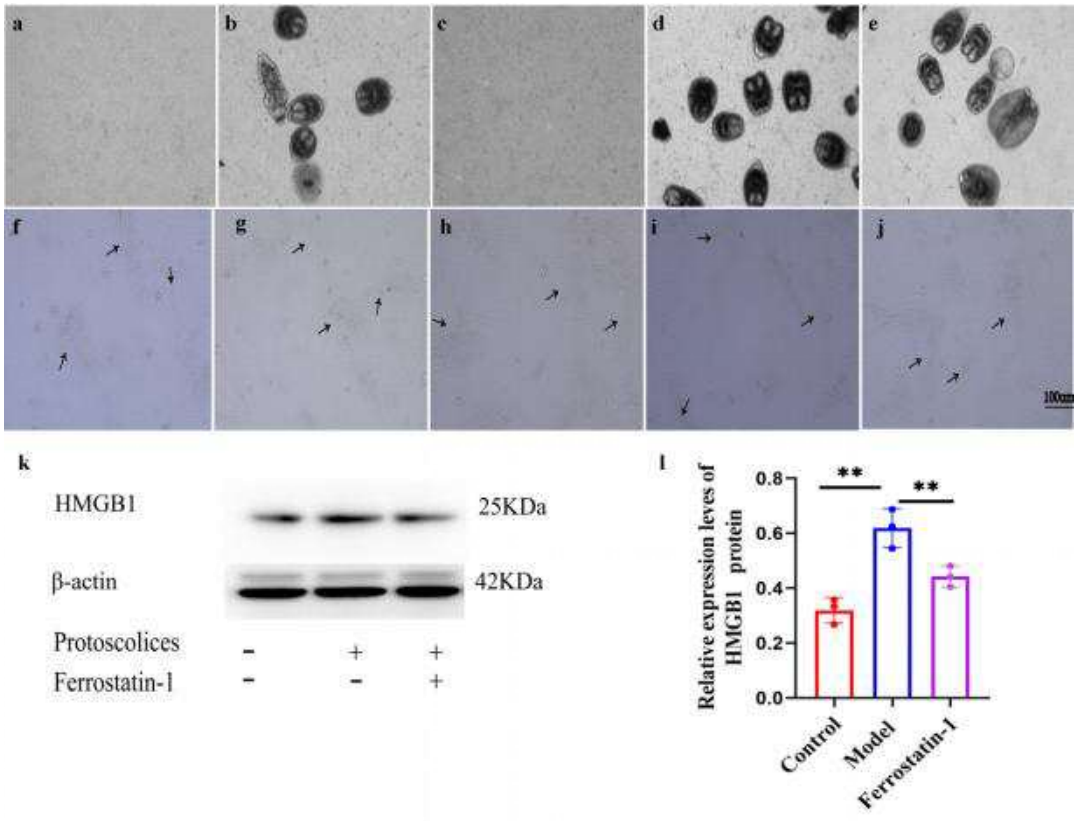


Fig 6. Morphological observation of BRL hepatocytes and HSC-T6 cells under different treatments in monoculture or co-culture, and the corresponding HMGB1 protein expression in BRL cells.

(a): Control group of BRL cells. (b): BRL cells with infection. (c): HMGB1 protein treatment group. (d): BRL cells with infection plus Fer-1 treatment. Purple arrows indicate BRL cells (scale bar: 100 μm). (e): BRL cells with infection plus GA treatment. (f): Control group of HSC cells. (g): Co-cultured HSC cells. (h): HMGB1 protein treatment group. (i): Co-cultured HSC cells plus Fer-1 treatment. (j): Co-cultured HSC cells plus GA treatment. White arrows indicate HSC-T6 cells (scale bar: 100 μm). (k): HMGB1 protein expression in BRL hepatocytes upon protoscolex infection and ferroptosis intervention. (l): Quantitative analysis of HMGB1 protein in BRL hepatocytes. n = 4 per group.

3.7 *E. granulosus* Induces HMGB1-Dependent Ferroptosis in BRL Hepatocytes

Biochemical and protein analyses were performed in control BRL cells, protoscolex-exposed cells, cells treated with recombinant HMGB1, and infected cells treated with Fer-1 or GA. *E. granulosus* exposure significantly increased intracellular Fe^{2+} (Fig. 7b), lipid peroxides (Fig. 7c), and MDA (Fig. 7f) and reduced GSH content (Fig. 7d) and SOD activity (Fig. 7e). Recombinant HMGB1 further intensified these changes (Fig. 7b-f), whereas Fer-1 and GA restored the measured indices toward control levels. Infection also increased HMGB1 (Fig. 7a) and TFRC expression (Fig. 7g, h) and reduced GPX4 expression (Fig. 7g, i). Fer-1 partially decreased HMGB1 abundance (Fig. 7a), consistent with feedback between ferroptotic injury and HMGB1 release, whereas GA more directly suppressed HMGB1 and reversed the associated ferroptotic profile. Collectively, these results showed that *E. granulosus*-induces ferroptosis in BRL hepatocytes and that HMGB1 amplifies this process.

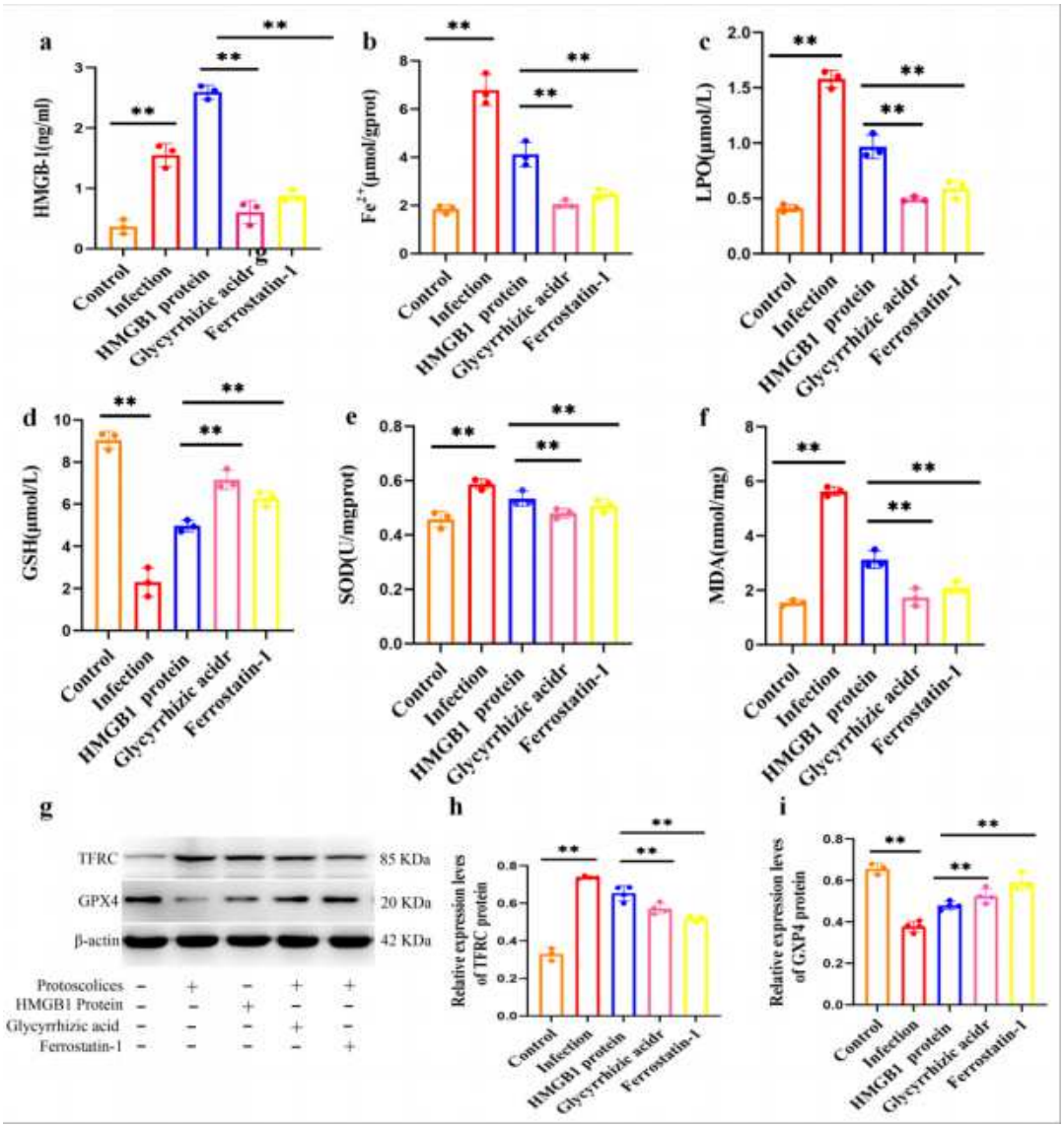


Fig 7. Effects of protoscolex infection on HMGB1 secretion, iron death-related oxidative stress markers (Fe^{2+}, LPO, GSH, SOD, MDA), and the protein expression of TFRC and GPX4 in BRL cells.

(a): HMGB1 secretion in BRL cells after protoscolex infection across different groups. (b): Fe^{2+} levels in BRL cells after protoscolex infection across different groups. (c): LPO levels in BRL cells after protoscolex infection across different groups. (d): GSH levels in BRL cells after protoscolex infection across different groups. (e): SOD levels in BRL cells after protoscolex infection across different groups. (f): MDA levels in BRL cells after protoscolex infection across different groups. (g): Expression of TFRC

and GPX4 proteins in BRL cells after protoscolex infection. Quantitative analysis of TFRC (h) and GPX4 (i) protein expressions in each group. n = 4 per group.

3.8 *E. granulosus* Infection Activates Fibrotic Signaling through HMGB1

Conditioned-medium experiments were used to determine whether HMGB1-dependent hepatocyte injury promoted HSC activation. Relative to controls, HSC-T6 cells exposed to conditioned medium from infected BRL cells exhibited increased Smad2/3 phosphorylation (Fig. 8a, c), alpha-SMA expression (Fig. 8a, d), and COL1A1 expression (Fig. 8a, e), whereas total Smad2/3 abundance was unchanged (Fig. 8a, b). Recombinant HMGB1 further enhanced these profibrotic responses (Fig. 8c-e). By contrast, treatment with GA or Fer-1 reduced Smad2/3 phosphorylation (Fig. 8c) and decreased alpha-SMA (Fig. 8d) and COL1A1 expression (Fig. 8e). Furthermore, the inflammatory signaling markers TLR4 (Fig. 8f) and MYD88 (Fig. 8g) were similarly modulated by these treatments. These findings indicate that HMGB1 promotes infection-associated HSC activation through TGF-β/Smad signaling and that both direct HMGB1 inhibition and ferroptosis blockade attenuate the profibrotic hepatocyte-HSC crosstalk.

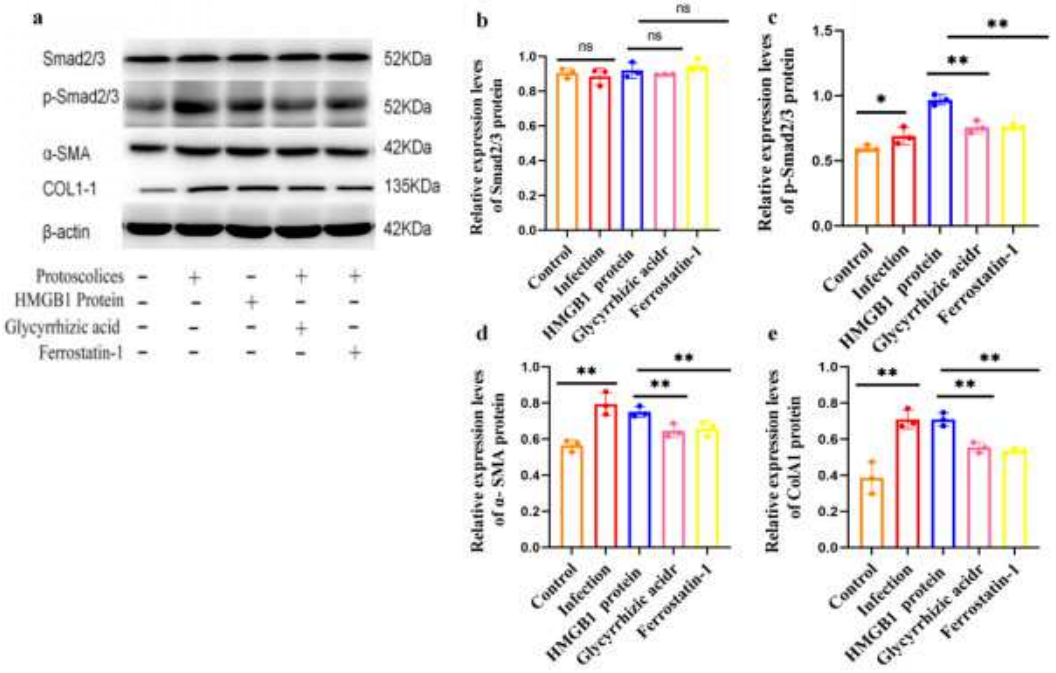


Fig 8. Effects of different treatments on the protein expression of Smad2/3, phosphorylated Smad2/3 (p-Smad2/3), α-SMA, COL1A1, TLR4, and MYD88.

(a): Protein expression levels of Smad2/3, p-Smad2/3, α-SMA, and COL1A1 in each group. The quantitative analysis of Smad2/3 (b), p-Smad2/3 (c), α-SMA (d), COL1A1 (e), TLR4 (f), and MYD88 (g) protein expressions. n = 4 per group.

4 Discussion

CE remains an important zoonotic disease with major consequences for public health and livestock production, and the liver is the organ most frequently affected[35,36]. Chronic hepatic infection is characterized by persistent inflammation, hepatocellular injury, and fibrotic cyst formation, but the molecular events that connect these processes are not fully understood[37,38]. By integrating naturally infected sheep tissues, an experimental rat model, and complementary hepatocyte-HSC culture systems, the present study identifies HMGB1 as an upstream regulator linking iron dysregulation and ferroptosis to inflammatory and fibrotic signaling during *E. granulosus* infection. The principal finding is that infection-induced HMGB1 release promotes a coordinated pathological program comprising TLR4/MYD88 activation, impaired antioxidant defense, hepatocyte ferroptosis, TGF-β/Smad signaling, and HSC activation.

Previous work, including our own, established that *E. granulosus* infection can induce hepatocyte ferroptosis[39,40], but the initiating signals and biological consequences of this response remained uncertain. In the present study, untreated infected rats developed multiple hepatic cystic lesions, marked histopathological injury, and extensive collagen deposition. Inhibition of either HMGB1 or ferroptosis reduced lesion burden and improved liver morphology, with HMGB1 inhibition producing the broader effect. Although these data do not establish a direct parasiticidal action, they suggest that HMGB1-dependent host injury and ferroptosis contribute to a tissue microenvironment

that favors lesion persistence and growth. Accordingly, modulation of the HMGB1-ferroptosis axis may simultaneously protect host tissue and restrict disease progression.

To clarify the key pathological features and optimal intervention timing during the transition from early hepatic injury to established fibrosis in echinococcosis, this study selected one month post-infection as the observation time point in the protoscolex-induced in vivo infection model. At this stage, hydatid cysts have begun to exert mechanical compression and secrete multiple factors that disrupt local hepatic architecture, but widespread and irreversible fibrotic remodeling has not yet occurred [41-43]. This transitional phase therefore provides an optimal window for intercepting early pro-fibrotic signals, enabling pharmacological intervention to genuinely modify disease progression rather than merely alleviating end-stage damage[44,45].

Although glycyrrhizic acid (GA) exhibits relatively weaker direct binding affinity for HMGB1 compared with other reported HMGB1 inhibitors, it was selected as the candidate drug based on several rationales[46]. First, GA is a well-characterized multi-target agent that, in addition to directly neutralizing HMGB1, exerts anti-inflammatory, antioxidant, and membrane-stabilizing effects[47]. Second, recent evidence indicates that GA regulates HMGB1 expression and secretion at both transcriptional and post-translational levels, thereby reducing extracellular HMGB1 abundance through mechanisms distinct from direct protein binding[48]. Third, its broader pharmacological profile allows simultaneous targeting of multiple key nodes within the HMGB1–ferroptosis–inflammation–fibrosis network, which is particularly advantageous given the multifactorial pathogenesis of parasitic liver injury. Finally, the established safety profile and clinical history of GA provide strong support for its translational application as a potential therapeutic agent[49].

Prussian blue staining was employed to spatially visualize the association between disordered iron metabolism and fibrosis. Iron-positive deposits were concentrated around hydatid cysts and in areas of hepatocellular injury, and these regions substantially overlapped with collagen-rich areas detected by Masson's trichrome staining. Both GA and Fer-1 reduced iron deposition in parallel with improvements in inflammatory infiltration and collagen accumulation. This spatial association, together with the biochemical evidence of increased Fe^{2+}, lipid peroxidation, and MDA, supports a close relationship among iron overload, ferroptosis, and fibrogenesis in infected liver tissue. Nevertheless, colocalization alone cannot prove causality, and future studies using cell-specific iron-tracing approaches will be required to define the cellular sources and temporal sequence of iron accumulation.

The mechanistic data further position HMGB1 upstream of ferroptosis and fibrosis. Infection increased HMGB1 in serum and liver tissue, upregulated TFRC, and downregulated SLC7A11 and GPX4, thereby favoring iron accumulation and lipid peroxidation. Direct HMGB1 inhibition corrected these abnormalities more comprehensively than ferroptosis inhibition, whereas Fer-1 partially reduced HMGB1 abundance. This pattern is consistent with a bidirectional relationship in which HMGB1 promotes ferroptosis and ferroptotic injury, in turn, amplifies HMGB1 release[33]. In parallel, infection activated TLR4/MYD88 and TGF-β/Smad signaling and increased alpha-SMA and COL1A1 expression. Suppression of these pathways by GA indicates that HMGB1 contributes not only to ferroptotic hepatocyte injury but also to inflammatory signaling and HSC activation[50].

The in vitro experiments corroborated the animal findings and clarified the cellular sequence of events. Protoscolex exposure increased HMGB1 release and induced a ferroptotic phenotype in BRL hepatocytes, whereas recombinant HMGB1 intensified iron

accumulation, lipid peroxidation, and GPX4 loss. Conditioned medium from injured hepatocytes activated HSC-T6 cells and increased Smad2/3 phosphorylation, alpha-SMA, and COL1A1. Both GA and Fer-1 attenuated these responses, indicating that hepatocyte-derived HMGB1 and ferroptotic stress contribute to paracrine activation of HSCs. These findings extend previous reports linking HMGB1 to ferroptosis and hepatic fibrogenesis by demonstrating their convergence in the context of *E. granulosus* infection.

Taken together, the results support a model in which mechanical and biochemical injury caused by *E. granulosus* promotes HMGB1 release from hepatocytes. Extracellular HMGB1 activates TLR4/MYD88-dependent inflammation and facilitates TGF-β/Smad-mediated HSC activation. Concurrently, HMGB1 disrupts iron and redox homeostasis, thereby promoting ferroptosis. Ferroptotic injury further increases HMGB1 release, generating a positive-feedback loop that sustains inflammation and fibrosis. The greater overall efficacy of GA relative to Fer-1 is consistent with HMGB1 acting upstream of several interconnected pathological pathways rather than exclusively within the ferroptotic response.

Several limitations should be acknowledged. First, the in vivo experiments were conducted in sheep and rats, and validation in human hepatic CE specimens is required to establish clinical relevance. Second, this study relied on pharmacological inhibition of HMGB1; in the absence of genetic approaches such as conditional knockout or CRISPR-based techniques, we could not definitively attribute the observed phenotypic effects to HMGB1 deficiency, nor could we exclude potential off-target effects of the drug. Third, parasite burden and cyst viability were not included as primary endpoints, leaving unresolved whether HMGB1 modulation directly affects parasite survival. Fourth, the dynamic changes of the HMGB1–ferroptosis axis across the acute and

chronic stages of infection were not examined, and longer-term follow-up and analysis will be needed to evaluate the progression of chronic fibrosis and determine whether early intervention can prevent progressive fibrotic remodeling. Fifth, the cellular sources of pathogenic HMGB1 were not thoroughly dissected; future studies employing cell type-specific HMGB1 knockout strategies will be necessary to determine whether hepatocytes, immune cells, or other parenchymal cell populations are the principal contributors. Sixth, although the conditioned medium experiments support crosstalk between hepatocytes and hepatic stellate cells, they do not fully elucidate the specific roles of macrophages and other immune cells within the infected liver microenvironment, and the physiological relevance of the co-culture system to the in vivo microenvironment remains limited.

Notably, the HMGB1–ferroptosis–fibrosis axis described here may not be limited to cystic echinococcosis but could also apply to other parasitic liver diseases[51]. In alveolar echinococcosis, caused by Echinococcus multilocularis, chronic infection similarly triggers robust inflammatory responses, progressive fibrosis, and hepatocellular injury, and recent studies suggest that ferroptosis plays an important role in parasite-mediated liver injury[39]. Likewise, in schistosomiasis, deposition of schistosome eggs in the liver can induce granulomatous inflammation and HMGB1 release, further promoting fibrotic progression through TLR4 and TGF-β signaling pathways[51]. These similarities suggest that the HMGB1–ferroptosis–fibrosis axis may represent a conserved host response mechanism to chronic parasitic liver injury, rather than a pathway unique to *E. granulosus* infection[18]. Nevertheless, direct comparative studies will be required to validate the generality and applicability of this axis across different parasitic etiologies.

5 Conclusions

HMGB1 is an upstream mediator linking *E. granulosus*-induced hepatocellular injury to ferroptosis, inflammation, and progressive hepatic fibrosis. Parasite-induced HMGB1 release disrupts iron homeostasis and antioxidant defense, activates TLR4/MYD88 and TGF-β/Smad signaling, and promotes HSC activation. Ferroptotic injury further enhances HMGB1 release, thereby sustaining a pathogenic positive-feedback loop. Pharmacological inhibition of HMGB1 produced broader protection than ferroptosis inhibition alone, reducing iron accumulation, lipid peroxidation, inflammation, collagen deposition, and lesion burden. These findings define an HMGB1-centered inflammation-ferroptosis-fibrosis axis and support HMGB1 as a potential host-directed therapeutic target for hepatic CE.

Supplementary Materials: No additional materials provided.

Acknowledgments: The authors thank Wuhan Servicebio Technology Co., Ltd. for their technical assistance with the preparation of pathological sections.

Funding: This research was funded by the Key Program of the Natural Science Foundation of Xinjiang Uygur Autonomous Region (Grant No. 2023D01D04), the Open Research Fund of the National Key Laboratory for Diagnosis and Treatment of Severe Zoonotic Infectious Diseases (Grant No. RCGHCRB202501).

Conflicts of Interest: All authors have no conflict of interest.

Ethics approval and consent to participate: All procedures were conducted in accordance with national and institutional guidelines for the care and use of laboratory animals and were approved by the Animal Care and Use Committee of Xinjiang Agricultural University (Approval No. 2022039; 10 December 2022).

Consent for publication: Not applicable.

Data Availability Statement: The data supporting the findings of this study are available from the corresponding author upon reasonable request.

Materials availability: This study did not generate new unique biological materials.

Code availability: Not applicable.

Author Contributions: Conceptualization, S.Z.; methodology, S.Z., S.L., and L.L.; , animal model construction, M.H. and Y.Y. ; data curation J.Z.; cellular experiments, X.W. and J.Y.; L.L.; formal analysis, S.Z.; writing-original draft preparation, S.Z.; writing-review and editing, S.Z.; supervision, S.Z.; funding acquisition, S.Z.; All authors have read and agreed to the published version of the manuscript.

References

[1] Hermassi MA, Guediche S, Zouaghi M*, et al.*(2024). Primary bilateral occipital hydatid cysts: Report of a rare entity. Int J Surg Case Rep,124(110464. https://doi.10.1016/j.ijscr.2024.110464.

[2] Mulpuri TC, Rajan YR, Sajja J*, et al.*(2024). A Case Series of Isolated Primary Hydatid Cyst of the Spleen. Cureus,16(6):e62252. https://doi.10.7759/cureus.62252.

[3] Abolhasani S, Babazadeh T, Maleki Chollou K*, et al.*(2025). Seroprevalence and risk factors associated with Cystic echinococcosis among nomadic, rural, and urban communities in Northwestern Iran. Parasitol Res,124(9):103. https://doi.10.1007/s00436-025-08555-4.

[4] Bazzi N, Baalbaki H, Njeim A*, et al.*(2024). Extrahepatic intraabdominal hydatid cyst: a case report. J Med Case Rep,18(1):399. https://doi.10.1186/s13256-024-04733-7.

[5] Fan S, Zhao X, Danqulamu*, et al.*(2022). Genetic diversity and haplotype analysis of yak and sheep echinococcal cysts isolates from the mitochondrial cox1 gene in parts of Tibet, China. Front Vet Sci,9(1016972. https://doi.10.3389/fvets.2022.1016972.

[6] Revés J, Delire B, Dongier A*, et al.*(2024). Cholangioscopic findings in complicated liver hydatid disease. Endoscopy,56(S 01):E766-E767. https://doi.10.1055/a-2387-4169.

[7] Shahid Y, Emman B, Abid S(2025). Liver parasites: A global endemic and journey from infestation to intervention. World J Gastroenterol,31(1):101360. https://doi.10.3748/wjg.v31.i1.101360.

[8] Tsukanov VV, Vasyutin AV, Tonkikh JL(2024). Parasites of the liver: A global problem? World J Gastroenterol,30(30):3554-3559. https://doi.10.3748/wjg.v30.i30.3554.

[9] Shamsan E, Chuanchuan L, Haining F(2026). Differential activation of hepatic stellate cells by Echinococcus multilocularis and Echinococcus granulosus protoscoleces. Parasitol Res. https://doi.10.1007/s00436-026-08681-7.

[10] Cao J, Chen J, Li H*, et al.*(2026). ROS-NLRP3 participates in the pyroptosis response of excretory-secretory products from protoscoleces of Echinococcus granulosus in hepatocytes. Sci Rep,16(1). https://doi.10.1038/s41598-026-45127-7.

[11] Wang H, Yu Q, Wang M*, et al.*(2023). Hepatic macrophages play critical roles in the establishment and growth of hydatid cysts in the liver during Echinococcus granulosus sensu stricto infection. PLoS Negl Trop Dis,17(11):e0011746. https://doi.10.1371/journal.pntd.0011746.

[12] Saftawy EAE, Ghallab MMI, Fadl HO*, et al.*(2026). Glycogen content and expression of CD10 and alpha-SMA in the microenvironment of viable human hepatic hydatid cysts. Gut Pathog,18(1). https://doi.10.1186/s13099-026-00797-6.

[13] Wang J, Li P, Li Y*, et al.*(2025). Exploring the mechanism and drug candidates of alveolar echinococcosis affecting liver fibrosis through analysis of existing microarray data. Acta Trop,263(107532. https://doi.10.1016/j.actatropica.2025.107532.

[14] Yang HC, Xing ZK, Shao H, *et al.*(2022). The expression of cytokeratin and apoptosis-related molecules in echinococcosis related liver injury. Mol Biochem Parasitol,248(111455. https://doi.10.1016/j.molbiopara.2022.111455.

[15] Hasanzadeh A, Beiromvand M, Rafiei A, *et al.*(2024). Expression of Matrix Metalloproteinases in Human Cystic Echinococcosis. Curr Mol Med,24(2):244-251. https://doi.10.2174/1566524023666230106163928.

[16] Taniyama O, Kumagai K, Kanmura S, *et al.*(2025). Continuous Intravenous Infusion of Hepatocyte Growth Factor Promotes the Development of a Fibrolytic Phenotype in Hepatic Macrophages and Stellate Cells in a Rat Model of Bile Duct Ligation. Hepatol Res,55(9):1307-1319. https://doi.10.1111/hepr.14227.

[17] Salzmann M, Resch U, Boccuni L, *et al.*(2025). Phytic acid impairs macrophage inflammatory response in Echinococcus multilocularis infection. Commun Biol,8(1):871. https://doi.10.1038/s42003-025-08283-6.

[18] Zhai S, Yang Y, Zhou Y, *et al.*(2025). Echinococcus granulosus-Induced Liver Damage Through Ferroptosis in Rat Model. Cells,14(5). https://doi.10.3390/cells14050328.

[19] Yang C, Wu A, Tan L, *et al.*(2023). Epigallocatechin-3-Gallate Alleviates Liver Oxidative Damage Caused by Iron Overload in Mice through Inhibiting Ferroptosis. Nutrients,15(8). https://doi.10.3390/nu15081993.

[20] Ishikawa K, Murao A, Murao T, *et al.*(2025). A MULTIPLE DAMAGE-ASSOCIATED MOLECULAR PATTERN-SCAVENGING COMPOUND OP18 ATTENUATES HEPATIC ISCHEMIA/REPERFUSION INJURY. Shock,64(2):265-271. https://doi.10.1097/shk.0000000000002624.

[21] Zeng W, Zhang X, Jiang Y*, et al.*(2025). Dualistic Roles of High Mobility Group Box 1 in Cancer and Inflammation. Cancer Med,14(23):e71455. https://doi.10.1002/cam4.71455.

[22] Wang CS, Kulaixi X, Zhou JR*, et al.*(2026). IL-1beta Blocker and Its Influence on Preserving Lung Tissues Sensitized by Echinococcus granulosus Sac Fluid by Regulating Macrophage Phenotypic Transformation. Curr Med Chem. https://doi.10.2174/0109298673425107251229063642.

[23] Chen Y, Wang C, Wu Y*, et al.*(2025). Magnesium Isoglycyrrhizinate Alleviates Alectinib-Induced Hepatotoxicity by Inhibiting Mitochondrial Damage-Mediated Pyroptosis. Drug Des Devel Ther,19(6219-6233. https://doi.10.2147/dddt.s523455.

[24] Luo G, Li H, Lu Q*, et al.*(2024). Effects of protoscoleces excretory-secretory products of Echinococcus granulosus on hepatocyte growth, function, and glucose metabolism. Acta Trop,249(107066. https://doi.10.1016/j.actatropica.2023.107066.

[25] Chen X, Zhao H, Tuohetali A*, et al.*(2025). EgG1Y162 protein from Echinococcus granulosus modulates the immune functions of mouse splenic lymphocytes and regulates Th9 cells. Int J Biol Macromol,322(Pt 1):146515. https://doi.10.1016/j.ijbiomac.2025.146515.

[26] Li Z, Xu M, Zhang Y*, et al.*(2026). Dibutyl phthalate exposure-induced AhR activation drives ferroptosis and HMGB1/TLR4-mediated inflammatory liver injury via NRF2-HO-1 signaling. Environ Pollut,398(128010. https://doi.10.1016/j.envpol.2026.128010.

[27] Jia YJ, Xiong S, Yao M*, et al.*(2024). HMGB1 inhibition blocks ferroptosis and oxidative stress to ameliorate sepsis-induced acute lung injury by activating the

Nrf2 pathway. Kaohsiung J Med Sci,40(8):710-721. https://doi.10.1002/kjm2.12851.

[28] Lv L, Wang Y, Lv X, *et al.*(2025). Involvement of HMGB1-mediated ferroptosis in systemic diseases. Front Cell Dev Biol,13(1676941. https://doi.10.3389/fcell.2025.1676941.

[29] Song Z, Han H, Ge X, *et al.*(2023). Deficiency of neutrophil high-mobility group box-1 in liver transplant recipients exacerbates early allograft injury in mice. Hepatology,78(3):771-786. https://doi.10.1097/hep.0000000000000346.

[30] Bai T, Guo HL, Wang F, *et al.*(2025). Gut microbiota and HMGB1/NLRP3/GSDMD inflammasome-dependent pyroptosis: mechanisms by physcion ameliorates alcoholic liver fibrosis. Front Pharmacol,16(1532590. https://doi.10.3389/fphar.2025.1532590.

[31] Li S, Mu WJ, Zhao ZA, *et al.*(2026). Hepatic Sirt2-PARP1-HMGB1 axis promotes exercise-mediated amelioration of MASH in mice. Sci China Life Sci,69(7):2342-2359. https://doi.10.1007/s11427-025-3241-0.

[32] Wei M, Zhang Y, Zhang H, *et al.*(2022). HMGB1 induced endothelial to mesenchymal transition in liver fibrosis: The key regulation of early growth response factor 1. Biochim Biophys Acta Gen Subj,1866(10):130202. https://doi.10.1016/j.bbagen.2022.130202.

[33] Li Y, Wang Q, Liao Z, *et al.*(2026). HMGB1-mediated enhancement of glycolysis activates hepatic stellate cells by inhibiting ferroptosis in alcoholic hepatic fibrosis. Stem Cell Res Ther,17(1). https://doi.10.1186/s13287-026-04970-1.

[34] Zhang J, Xie Z, Zhu X, *et al.*(2025). New insights into therapeutic strategies for targeting hepatic macrophages to alleviate liver fibrosis. Int Immunopharmacol,158(114864. https://doi.10.1016/j.intimp.2025.114864.

[35] Liu B, Chen Q, Cai J*, et al.*(2025). The Effect of Lamb Vaccination Against Echinococcosis on the Scale of Livestock Farming in Northwestern China. Vet Med Sci,11(2):e70273. https://doi.10.1002/vms3.70273.

[36] Jamiel A, Mohamed S, Alobaid NK*, et al.*(2026). Ruptured Pericardial Hydatid Cyst Causing Mitral Annulus Distortion With Severe Mitral Regurgitation and Tamponade-like Symptoms: A Case Report. Am J Case Rep,27(e950600. https://doi.10.12659/ajcr.950600.

[37] Liu T, Pu G, Wang L*, et al.*(2025). LncRNA gm40262 promotes liver fibrosis and parasite growth through the gm40262-miR-193b-5p-TLR4/Col1alpha1 axis. mBio,16(4):e0228724. https://doi.10.1128/mbio.02287-24.

[38] Ko C, Cheng CC, Mistretta D*, et al.*(2025). SARS-CoV-2 Productively Infects Human Hepatocytes and Induces Cell Death. J Med Virol,97(1):e70156. https://doi.10.1002/jmv.70156.

[39] Chen J, Ma Y, Fan B*, et al.*(2025). Targeted inhibition of METTL3 reprograms alveolar echinococcosis progression: attenuating ferroptosis by downregulating ACSL4 and reversing macrophage M2 polarization. Int Immunopharmacol,167(115660. https://doi.10.1016/j.intimp.2025.115660.

[40] Mu X, Zhao C, Li L*, et al.*(2025). Echinococcus granulosus induces mitophagy and mitochondrial dysfunction in AML12 hepatocytes. Diagn Microbiol Infect Dis,113(2):116952. https://doi.10.1016/j.diagmicrobio.2025.116952.

[41] Yuqing C, Yaxin S, Ying W*, et al.*(2026). Dynamic changes of innate lymphoid cells in the liver of mice infected with Echinococcus multilocularis during the progression of hepatic fibrosis. CHINESE JOURNAL OF PARASITOLOGY AND PARASITIC DISEASES,44(2):174-181. https://doi.10.12140/j.issn.1000-7423.2026.02.004.

[42] Hongbin Z, Bowen S, Xue Z*, et al.*(2025). Changes of ADAM metallopeptidase domain 23 expression in hepatic fibrosis of mice infected with Echinococcus multilocularis. CHINESE JOURNAL OF PARASITOLOGY AND PARASITIC DISEASES,43(6):777-785. https://doi.10.12140/j.issn.1000-7423.2025.06.005.

[43] LI W-d, WEN H, HOU J*, et al.*(2021). Role of extracellular matrix protein 1 in the liver fibrosis induced by Echinococcus multilocularis infection in mice. CHINESE JOURNAL OF PARASITOLOGY AND PARASITIC DISEASES,39(3):296-303. https://doi.10.12140/j.issn.1000-7423.2021.03.002.

[44] Zhai S, Yang Y, Hu M*, et al.*(2026). Effect of LY2109761 on TGF-β1/TGFβRI/Smad Pathway and Hepatic Fibrosis Cysts Formation in Rats Infected with Echinococcus granulosus: an In Vitro and In Vivo Study. Acta Parasitol,71(4). https://doi.10.1007/s11686-026-01324-y.

[45] Wu B, Yang Y, Cheng S*, et al.*(2025). Activation of the Wnt signaling pathway and its role in epithelial-mesenchymal transition and hepatic fibrosis in alveolar echinococcosis. Front Cell Infect Microbiol,15(1583802. https://doi.10.3389/fcimb.2025.1583802.

[46] Mollica L, De Marchis F, Spitaleri A*, et al.*(2007). Glycyrrhizin binds to high-mobility group box 1 protein and inhibits its cytokine activities. Chem Biol,14(4):431-441. https://doi.10.1016/j.chembiol.2007.03.007.

[47] Li JY, Cao HY, Liu P*, et al.*(2014). Glycyrrhizic acid in the treatment of liver diseases: literature review. Biomed Res Int,2014(872139. https://doi.10.1155/2014/872139.

[48] Wu CX, He LX, Guo H*, et al.*(2015). Inhibition effect of glycyrrhizin in lipopolysaccharide-induced high-mobility group box 1 releasing and expression from

RAW264.7 cells. Shock,43(4):412-421. https://doi.10.1097/shk.0000000000000309.

[49] Tian X, Gan W, Nie Y*, et al.*(2021). Clinical efficacy and security of glycyrrhizic acid preparation in the treatment of anti-SARS-CoV-2 drug-induced liver injury: a protocol of systematic review and meta-analysis. BMJ Open,11(7):e051484. https://doi.10.1136/bmjopen-2021-051484.

[50] Zhang Z, Lin C, Peng L*, et al.*(2012). High mobility group box 1 activates Toll like receptor 4 signaling in hepatic stellate cells. Life Sci,91(5-6):207-212. https://doi.10.1016/j.lfs.2012.07.009.

[51] Zhong H, Gui X, Hou L*, et al.*(2022). From Inflammation to Fibrosis: Novel Insights into the Roles of High Mobility Group Protein Box 1 in Schistosome-Induced Liver Damage. Pathogens,11(3). https://doi.10.3390/pathogens11030289.